

Profile and contact force estimation of cable-driven continuum robots in presence of obstacles

K.P. Ashwin^a, Soumya Kanti Mahapatra^b, Ashitava Ghosal^{b,*}

^aDepartment of Mechanical Engineering, BITS Pilani K.K. Birla Goa Campus, Goa, 403726, India

^bDepartment of Mechanical Engineering, Indian Institute of Science, Bangalore, 560012, India

Abstract

Accurate prediction of shape and contact forces significantly improves the performance of a continuum robot during its operation in obstacle-laden environments. This paper presents an optimization-based mathematical framework to predict the bending profile of a cable-driven continuum robot in presence of obstacles. The kinematics model is derived from the concept of strain energy minimization and can easily incorporate obstacles as inequality constraints in the optimization routine. The location of point of contact can be identified by observing the Lagrange multipliers of the inequality constraints. Using the kinematics model and the principle of virtual work, a method to estimate the reaction forces at contact is proposed. The model shows high accuracy, with RMS error of 1.35 mm in prediction of the pose for experiments conducted on a 180 mm long robot prototype. Validatory experiments are also conducted on the prototype by imposing contact at different locations on the robot. In all cases, the average error in predicting the contact force is found to be less than 0.9 grams for applied loads ranging from 50 to 350 grams.

Keywords: continuum robot, cable driven, tendon driven, kinematics, contact force estimation

1. Introduction

A continuum robot, as opposed to rigid link robot is characterized by a continuous elastic structure which is deformed using different actuation techniques (Robinson and Davies, 1999). Continuum robots are convenient for situations where compliance is preferred such as during human-robot interactions or handling delicate objects. Due to the hyper-redundancy in the continuum robot, they are also suitable for operations in inaccessible areas as well as for obstacle avoidance problems. A class of continuum robots which are actuated using cables (or tendons) are of particular interest due to their simplicity in design and miniaturizability (Walker, 2013; Walker et al., 2016). A typical cable-driven continuum robot (CCR) consists of a slender elastic *backbone* on which a set of disks are fixed with constant spacing (refer Fig. 1a). Through the holes in the disks,

*Corresponding author

Email addresses: ashwinp@goa.bits-pilani.ac.in (K.P. Ashwin), soumyam@iisc.ac.in (Soumya Kanti Mahapatra), asitava@iisc.ac.in (Ashitava Ghosal)

Preprint submitted to Mechanism and Machine Theory

March 10, 2021

cables are routed along the length of the backbone and are terminated at the end-disk. By pulling the cable from the base, a moment arm is generated at the tip, causing the CCR to bend.

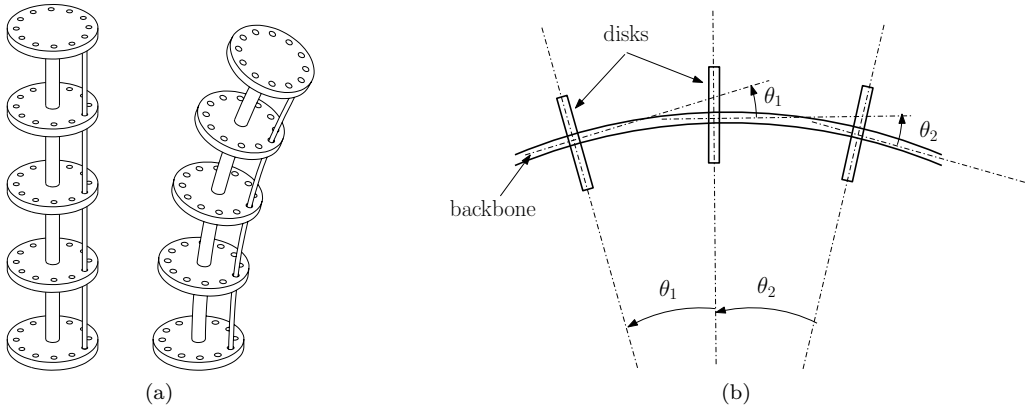


Figure 1: (a) Cable-driven continuum robot with cables terminating at the tip. (b) Slope angle is equivalent to the change in angle between consecutive disks of CCR.

Accurate mathematical models for the physics of CCR is of great interest since they can be used in robot design and control. A good mathematical model for CCR analysis also helps to understand the behaviour of the robot during contact with its environment. Since CCRs are generally light-weight and their applications involve slow movements of the robot, study of statics and kinematics are usually prioritized over dynamics. A detailed review of such analyses can be found in the works of Webster III and Jones (2010), Chirikjian (2015), Rao et al. (2021) etc. In Rao et al. (2021), the authors classified the modelling approaches as distributed and lumped models based on the type of backbone parametrization and their modelling assumptions. In distributed models, the backbone is considered as a 3-D curve which is represented using a single parameter, usually the normalized arc-length of the curve. For such models, kinematic analysis is conducted by representing the rate of change of position and rotation of backbone in the Frenet-Serret frame as functions of strain variables (Webster III and Jones, 2010). For lumped model analysis, the continuum backbone is discretized into finite segments and variables such as Denavit-Hartenberg parameters or joint co-ordinates are used for parameterizing the backbone curve (Camarillo et al., 2008; Mishra et al., 2018).

For static analysis of distributed models, the forces and moments distributed in the entire length of the robot are first accounted for. Different modelling considerations such as cable routing characteristics (Rucker and Webster III, 2011) and additional forces (Do et al., 2015) add different levels of complexity to these formulations. For straight-routed robots, Euler-Bernoulli beam theory is used for constitutive relations (Dehghani and Moosavian, 2013) while for generally-routed robots, Cosserat-rod theory is used (Rucker and Webster III, 2011). The solution to these boundary-value problems are usually computed by numerical integration. For static analysis of lumped models, a pseudo-rigid body approach is commonly used, where the backbone is considered as a series of rigid links connected using torsional springs (Khoshnam and Patel, 2013), (Venkiteswaran

et al., 2019). The internal torques of the backbone segments is related to the applied torques (and forces) by means of the robot’s Jacobian where the stiffness of springs and the optimal lengths of segments are determined from experiments. In the distributed models, external force constraints are incorporated as boundary conditions for the governing differential equations (Ryu et al., 2020). In the lumped model, the kinematic and static constraints are directly applied by specifying the position or load at the individual segments (Venkiteswaran et al., 2019). In both the cases, prior knowledge of the location of contact between the CCR and the object is necessary so that either the differential equations or the solution procedure can be modified accordingly.

In this paper, we present an optimization-based framework for solving the kinematics of CCR in presence of obstacles where prior knowledge on the location of contact is not necessary. The framework is an improved version of the model developed in Ashwin and Ghosal (2021), where the CCR is parametrized as a lumped model comprising of a series of adjoined hypothetical 4-bar linkages. An updated optimization framework is developed, where the external obstacles can be added as constraints to the global optimization routine. The accuracy of predicting the pose of a CCR is verified from experiments and a method to identify contact location is demonstrated. By utilizing the developed kinematics model and by employing the principle of virtual-work, a method to estimate the contact forces on obstacles is presented. The method is experimentally verified and it is shown that the contact force can be estimated with a maximum error of 0.75%. The rest of the paper is organized as follows: In section 2, the optimization-based kinematics formulation starting from strain energy minimization principles is introduced. The extension of kinematics formulation to include obstacles and identification of contact location is discussed in section 3. Accuracy of the method is demonstrated through validity experiments. In section 4, contact force estimation using virtual work principle is presented. The discussions on the developed framework and conclusions of the paper are presented in sections 5 and 6, respectively.

2. Optimization-based kinematics model

In this section, we derive the optimization-based kinematics of CCR from the principle of strain energy minimization. For the kinematic analysis shown in the sections 2, 3 and 4, we consider a CCR actuated using only one cable which is routed parallel to the backbone.

In most of the CCR designs, the backbone is a long slender member whose deformation can be considered as an elastic beam undergoing bending deformation. Upon application of an external load, the member deforms such that its strain energy is minimum at the static equilibrium. This is equivalent to the expression

$$\min_{\phi} \int_0^{L_0} B \left(\frac{d\phi}{ds} \right)^2 ds \quad (1)$$

where ϕ is the slope angle, s is the arc-length parameter, B is the flexural rigidity and L_0 is the length of the backbone. In a finite difference form, the above equation can be written as

$$\min_{\Delta\phi} \sum_{i=1}^n B \left(\frac{\Delta\phi}{\Delta s} \right)^2 \delta s \quad (2)$$

Assuming that the backbone is discretized into equal number of segments and the material is isotropic, the above equation becomes

$$\min_{\Delta\phi} C \sum_{i=0}^n (\Delta\phi)^2 \quad (3)$$

where C is a constant. Hence, the CCR in static equilibrium will have a deformed profile where the sum of squares of the change in slope angles is minimized – modulo a constant. Since the construction of CCR ensures that the disk is always perpendicular to the backbone, the change in slope angle is also equivalent to the angle between the two consecutive disks (refer Fig. 1b). Hence, minimization of the latter ensures that the kinematic criterion for the backbone with perpendicular disks is met. When the CCR is actuated, the above condition is augmented by the kinematic constraints imposed by the length of the cables in the segment and the size of the guiding disks. With these added constraints, we can uniquely identify the profile of the actuated CCR.

For mathematically representing the minimization problem and the constraints, the following nomenclature is assigned (refer Fig. 2):

- The backbone and cables are discretized into n segments, each comprising of a closed loop made of a backbone segment, top disk, cable segment and a bottom disk.
- The segment lengths of backbone and cable are l_0 and l_a respectively and they take the values $l_0 = l_a = L_0/n$ in the unactuated state.
- Distance between the cable and the backbone is fixed along the disk and is given by the constant a which is the same for all the disks.

For analysis, the numbering of segments start from bottom, where bottom most disk has the index $i = 0$, and the disk at the tip of the robot has the index $i = n$. The vertices of the loop in the i^{th} segment are termed $(\mathbf{X}_0^i, \mathbf{X}_a^i, \mathbf{X}_a^{i+1}, \mathbf{X}_0^{i+1})$ in the clockwise direction starting from the bottom left vertex. When the CCR is actuated, the linkage l_a reduces its length from $\frac{L_0}{n}$ to $\frac{L_0 - l}{n}$ where l is the amount by which the cable is pulled. The loop deforms as shown in Fig. 2 and the quantities $\mathbf{X}_{(\cdot)}^i$ change to $\mathbf{x}_{(\cdot)}^i$.

Using the aforementioned nomenclature, the optimization problem can be written as:

$$\arg \min_{\mathbf{x}_0, \mathbf{x}_a} \sum_{i=0}^{n-1} \left(\arccos \left(\left(\frac{\mathbf{x}_0^{i+1} - \mathbf{x}_a^{i+1}}{\|\mathbf{x}_0^{i+1} - \mathbf{x}_a^{i+1}\|} \right) \cdot \left(\frac{\mathbf{x}_0^i - \mathbf{x}_a^i}{\|\mathbf{x}_0^i - \mathbf{x}_a^i\|} \right) \right) \right)^2$$

Subject to:

$$\begin{aligned} \|\mathbf{x}_0^i - \mathbf{x}_0^{i-1}\| &= l_0 \\ \|\mathbf{x}_a^i - \mathbf{x}_a^{i-1}\| &= l_a \\ \|\mathbf{x}_0^i - \mathbf{x}_a^i\| &= a, \quad i = 1, 2, 3, \dots, n \end{aligned} \quad (4)$$

Given data: l_0, l_a, a ;

where the variables without segment index represent the arrays $\mathbf{x}_{(\cdot)} = [\mathbf{x}_{(\cdot)}^1, \mathbf{x}_{(\cdot)}^2, \dots, \mathbf{x}_{(\cdot)}^n]$ etc.

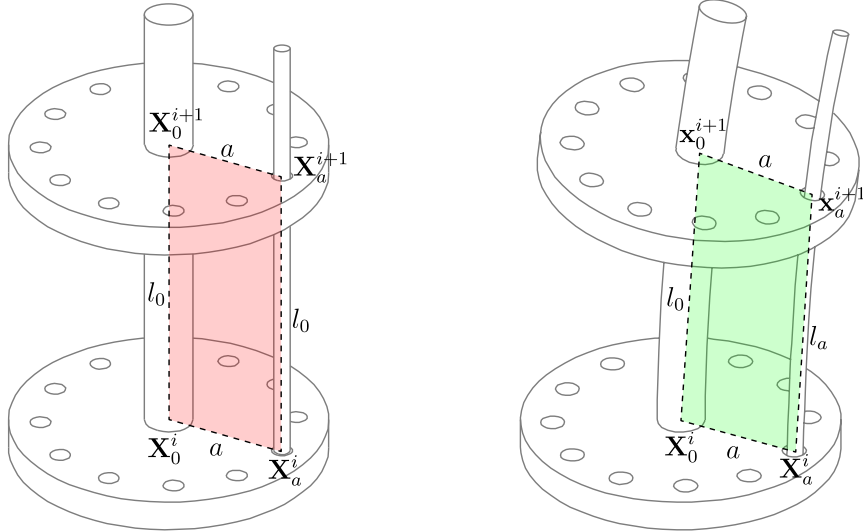


Figure 2: Nomenclature and variables used in optimization

The above optimization problem is solved as a global optimization problem with constraints. This approach allows us to add global constraints to the minimization routine and can be used for obstacle avoidance (Menon et al., 2013). The results presented in sections 3 and 4 presents the details of this approach, numerical results and experimental validation of the numerical results.

2.1. Experimental set-up and comparison of results

To validate the formulation, the equation (4) is solved and compared with the profile of a robot prototype. The prototype (Fig. 3a) is 3D printed using ABS material and is 183 mm long with 10 spacer disks of 3 mm each attached at equal spacing.

This fixes the length l_0 as 20 mm. The disks have 12 holes of 1.3 mm diameter arranged in a the periphery of a circle with 8 mm radius. Hence, $a = 8$ mm for this robot. For the cable, nylon cord of diameter 0.5 mm is used and is attached to the topmost disk. The deformation of the robot is captured using a camera positioned perpendicular to the plane of bending, and the profile obtained from theoretical formulation is super-imposed on the captured images for comparison. Fig. 3b shows the actual deformation of the robot prototype with the simulated results superimposed on the same.

The red markers show the values of \mathbf{x}_0 and the blue markers show the values of \mathbf{x}_a . The optimization problem was solved using `fmincon` routine in MATLAB considering 18 segments (19 nodal co-ordinates). A total of 76 optimization variables are solved at once which took about 2.6 seconds per iteration in an Intel processor at 2.00 GHz and 8 GB RAM. For all the experiments, the cable is pulled by a certain amount, and the reduction of lengths of each cable segments are assumed to be equal, i.e., $l_a = l_0 - \frac{l}{n}$ for all the segments. Cable displacement is computed from photos using image processing. The root mean square of the difference between the value of \mathbf{x}_0 obtained experimentally

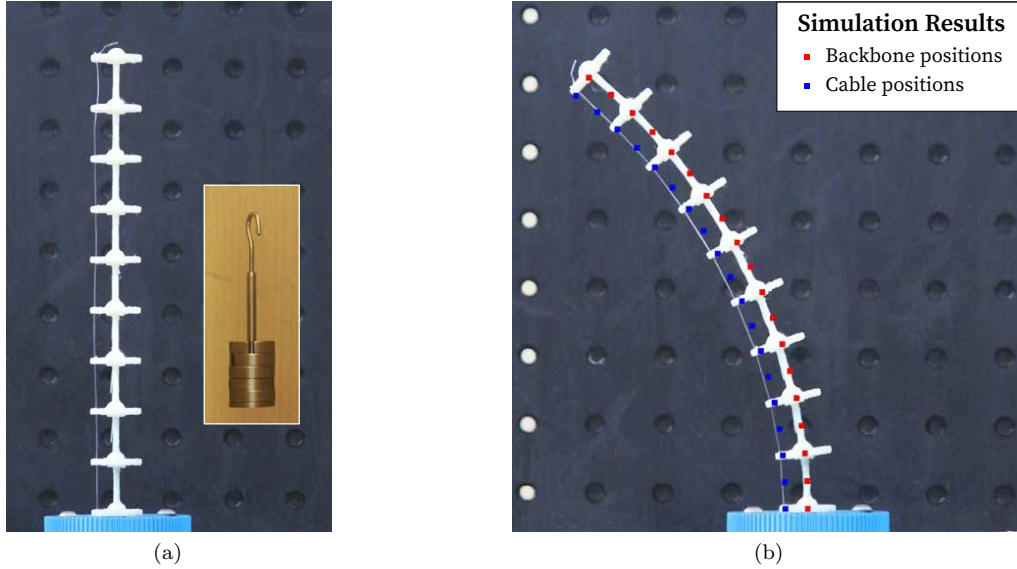


Figure 3: (a) Fabricated prototype of CCR with single cable passing through the disks. The cable is terminated at the topmost disk. The CCR is loaded by hanging known weights from below, as shown in the inset. (b) CCR bending results with simulated plot superimposed on experimental photo

and theoretically is used as a measure of accuracy of estimation. For the results shown in Figure 3b, the RMS error is 1.35 mm, which is 0.75% of the length of the CCR.

3. Kinematics model with obstacles

For the constrained global optimization problem, obstacle avoidance can be achieved by adding extra constraints in addition to the equality constraints in (4) (Menon et al., 2013; Ashwin et al., 2020). For obstacle avoidance, the problem can be reformulated as:

$$\arg \min_{\mathbf{x}_0, \mathbf{x}_a} \sum_{i=0}^{n-1} \left(\arccos \left(\left(\frac{\mathbf{x}_0^{i+1} - \mathbf{x}_a^{i+1}}{\|\mathbf{x}_0^{i+1} - \mathbf{x}_a^{i+1}\|} \right) \cdot \left(\frac{\mathbf{x}_0^i - \mathbf{x}_a^i}{\|\mathbf{x}_0^i - \mathbf{x}_a^i\|} \right) \right) \right)^2$$

Subject to:

$$\begin{aligned} \|\mathbf{x}_0^i - \mathbf{x}_0^{i-1}\| &= l_0 \\ \|\mathbf{x}_a^i - \mathbf{x}_a^{i-1}\| &= l_a \\ \|\mathbf{x}_0^i - \mathbf{x}_a^i\| &= a, \quad i = 1, 2, 3, \dots, n \\ \mathbf{f}(\mathbf{x}_0) &\succeq 0 \\ \mathbf{f}(\mathbf{x}_a) &\succeq 0 \end{aligned} \tag{5}$$

Given data: $l_0, l_a, a, \mathbf{f}(\mathbf{x})$ where $\mathbf{f}(\mathbf{x})$ is the function for boundaries of the obstacles¹. For example, if $\mathbf{f}(\mathbf{x}) =$

¹The generalized inequality symbol \succeq is used to represent vector inequalities

$(\mathbf{x} - x_c)^2 + (\mathbf{y} - y_c)^2 - r_c^2$, then the discrete points of the backbone and the cable will always lie outside a circle with center (x_c, y_c) and radius r_c .

As mentioned in section 1, this method does not require explicit knowledge of the location of point of contact in the CCR. In fact, the location of the point of contact can be found by observing the Lagrange parameters of the constrained optimization problem. Wherever the nodal co-ordinates violate the non-linear constraint, the Lagrange multipliers turn non-zero and hence can be used as an identifier to determine the nodes which are in contact.

3.1. Experimental validation

The solution to the optimization problem (5) is compared with experimental results for a single obstacle in 2D plane and is shown in Fig. 4a.

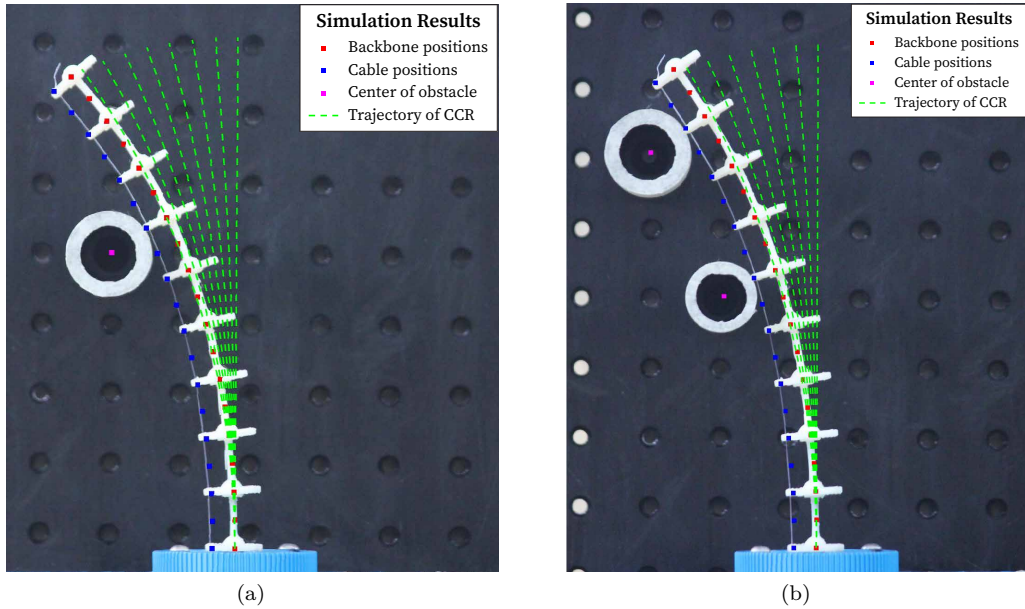


Figure 4: Resulting deformation for CCR in contact with (a) one obstacle, (b) two obstacles.

An object with circular cross-section of diameter 30 mm is fixed at a distance of 44 mm in the X direction and 104 mm in the Y direction from the base. The proposed formulation correctly predicts the pose of the CCR with an error of 0.58% of the total length of the CCR. In Fig. 4b, the numerical solution is compared with experimental profile for CCR in contact with two obstacles. The first obstacle of diameter 25 mm is kept at a distance of 33 mm and 89 mm from the base in the x and y directions respectively, the second obstacle of diameter 30 mm is kept at 59 mm and 140 mm from the base in the x and y directions respectively. The error in this case is 0.58% of the total length of the CCR. In both cases, computation time is about 4 seconds.

In Matlab, the Lagrange multipliers corresponding to the inequality constraint can be obtained from the output of the `fmincon` routine. Fig. 5 show the Lagrange multipliers

corresponding to the inequality constraints $f_1(\mathbf{x}_a) \geq 0$ and $f_2(\mathbf{x}_a) \geq 0$, respectively. The peak of the curves occur at the nodes 11 and 17 which corresponds to the disks 6 and 9 from the bottom. These are the actual contact locations as can be observed from Fig. 4b.

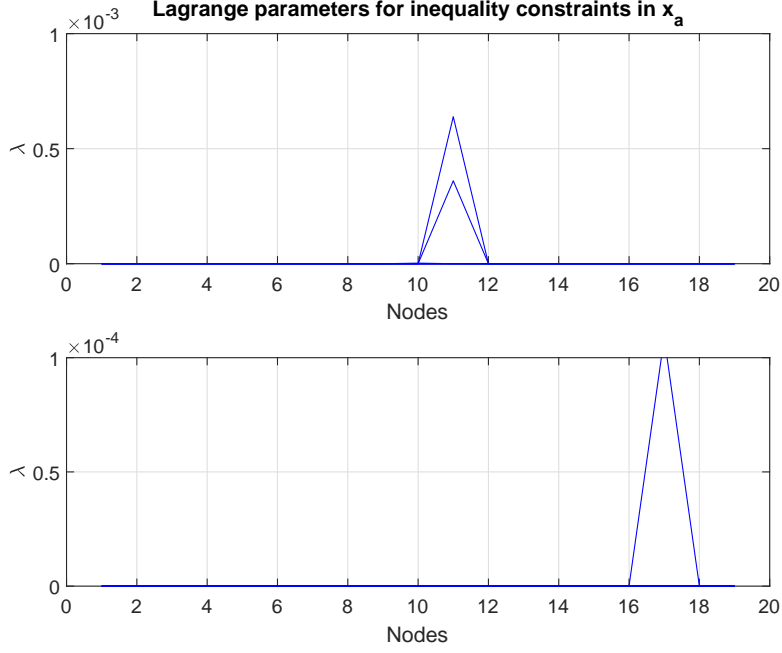


Figure 5: Contact position estimation from Lagrange multipliers

4. Estimating contact forces using the kinematics model

From the previous section, we see that the optimization-based kinematics formulation is able to predict the pose of the CCR with maximum error of 0.75% of the total length of the CCR and also determine the point of contact. In this section, we show how the results from the kinematics can be used to estimate the contact forces using the principle of virtual work.

The position and orientation of the tip of the robot (x_e, y_e, θ_e) can be represented as a function of the change in cable length:

$$x_e = f_x(l), \quad y_e = f_y(l), \quad \theta_e = f_\theta(l) \quad (6)$$

where the functions f_x, f_y and f_θ can be obtained from the kinematics model. The variational displacements will be

$$\delta x_e = f'_x \delta l, \quad \delta y_e = f'_y \delta l, \quad \delta \theta_e = f'_\theta \delta l \quad (7)$$

where $f'_{(\cdot)} = \frac{df(\cdot)}{dl}$. When the tip of CCR is constrained due to external object, a set of reaction forces and moment (P_x, P_y, M_e) as well as (R_x, R_y, M_r) are generated at the tip and the base respectively (see Fig. 6). Let $\delta x, \delta y$, and $\delta \theta$ denote the virtual displacement

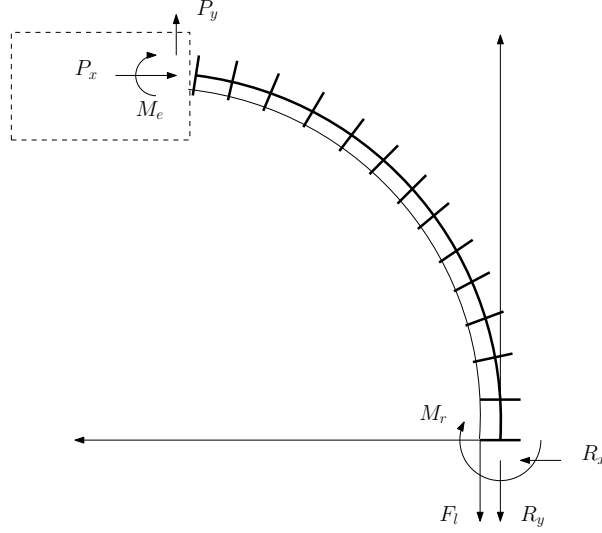


Figure 6: Free body diagram of the CCR with obstacle in contact at the tip

field corresponding to the reaction forces at the base. The virtual displacement at the tip due to (P_x, P_y, M_e) will be $(\delta x + f'_x \delta l, \delta y + f'_y \delta l, \text{ and } \delta \theta + f'_\theta \delta l)$ respectively. By invoking the principle of virtual work, we get

$$-R_x \delta x - R_y \delta y - M_r \delta \theta + P_x (\delta x + f'_x \delta l) + P_y (\delta y + f'_y \delta l) + M_e (\delta \theta + f'_\theta \delta l) = 0 \quad (8)$$

Regrouping the terms,

$$(-R_x + P_x) \delta x + (P_y - R_y) \delta y + (-M_r + M_e) \delta \theta + (P_x f'_x + P_y f'_y + M_e f'_\theta) \delta l = 0 \quad (9)$$

from which we obtain the static equilibrium equations:

$$\begin{aligned} R_x &= P_x, & R_y &= P_y, & M_r &= M_e \\ P_x f'_x + P_y f'_y + M_e f'_\theta &= 0 \end{aligned} \quad (10)$$

From the kinematics, we get the functions f'_x, f'_y , and f'_θ . The component $M_e = M_r$ is the moment generated at the tip of the robot due to the applied load F_l . i.e, $M_e = a \times P_l$ (Gravagne et al., 2003). Hence, by knowing one of the force components F_x or F_y , the other can be calculated.

4.1. Experimental validation

The values for the tip displacement in x, y and θ directions as functions of l can be obtained from the kinematics analysis as shown in Fig. 7. Linear curves are fitted in

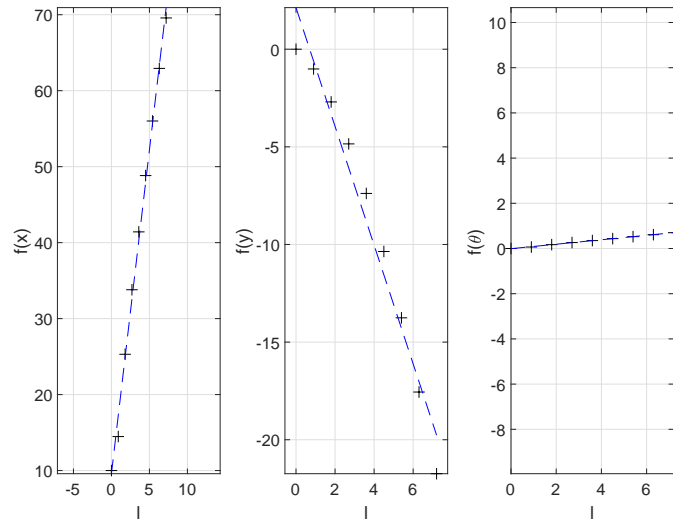


Figure 7: Tip displacement in X, Y, θ directions as function of cable displacement

this profile whose slopes directly give the values of f'_x, f'_y , and f'_θ . Fig. 8 shows the experimental set-up where a load cell is kept at 26 mm from the backbone in the X direction and 127 mm from the base. As the CCR is pulled, the third disk from the top

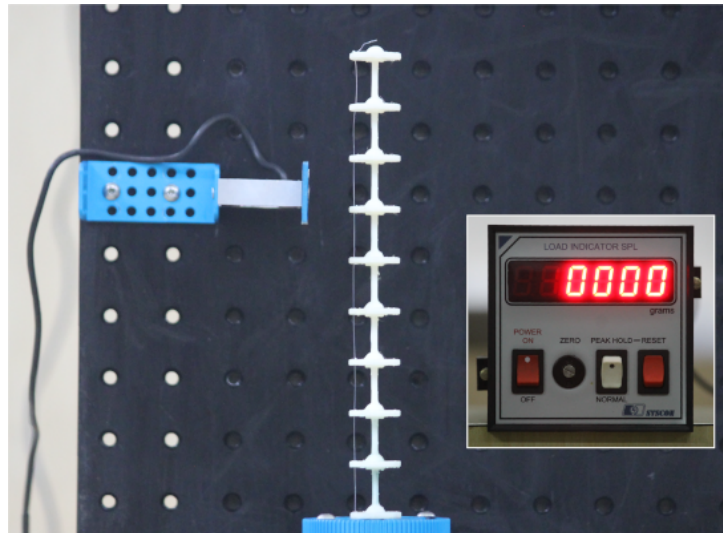


Figure 8: Experimental set-up for measuring contact forces. Force value is obtained from the meter in grams as shown in the inset

comes into contact with the load cell and the force readings in X direction are directly observed from the meter. The datum for the applied load F_l is set to the value where the CCR is in contact with the load cell. As per the experimental set-up, the component F_y should be zero since the direction is not constrained and the tip is allowed to slide along the surface of the load cell. However, this is not the case due to friction between the load cell and the CCR. In order to account for this force, we assume the vertical force $P_y = \mu P_x$. Then from equation 10, we get

$$P_x = -\frac{aP_l f'_\theta}{\mu f'_y + f'_x} \quad (11)$$

The quantity μ is found out from one experimental data point and is used throughout the rest of this paper.

Fig. 9 shows the experimental results with the numerical results superimposed on the figure. Since the load cell imposes constraint in the X -direction only on the 15th node,

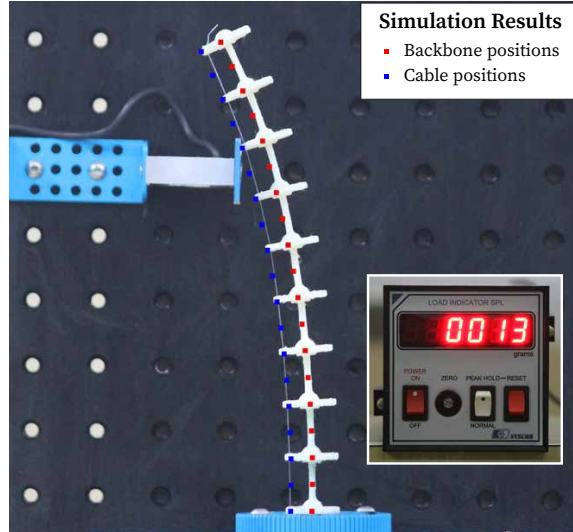


Figure 9: Contact force and kinematics for obstacle contact at third disk from the top

the constraint equation is prescribed as

$$\mathbf{f}(x) = d - x_a^{[15]} \quad (12)$$

where $x_a^{[15]}$ is the x-component of the position vector \mathbf{x}_a at the 15th node and d is the distance between the backbone and the load cell. The values of forces obtained experimentally is plotted alongside the numerical solution in Fig. 10a.

The experimental results accurately match with the theoretical results with maximum error less than 0.5g. More experiments are conducted by varying the distance between the backbone and the load cell and the comparison between experimental and theoretical values are tabulated in Table 1².

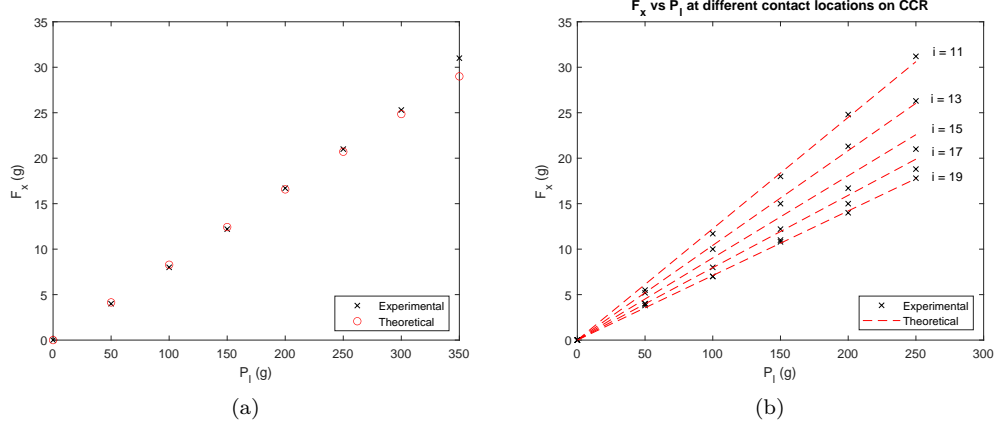


Figure 10: Comparison between experimental and theoretical values of contact forces (a) when the third disk from the top touches the load cell, (b) for different contact points in CCR.

Table 1: Experimental vs theoretical values of contact force when load cell is placed at d distance from the centre of backbone

P_l (g)	Experimental F_x (g)				Theoretical F_x (g)
	$d = 24$ mm	$d = 31$ mm	$d = 36$ mm	$d = 51$ mm	
50	3	4	3	3	3.5
100	7	7	7	7	7.1
150	10.2	10.8	10	10	10.7
200	13.7	14	14	14	14.2
250	17	17.8	17	17	17.8
300	20.2	21	20.5	21	21.3
350	23	24.8	23.8	24	24.9

From experiments, the value of force is observed not to appreciably change with offset d . Further experiments are conducted by changing the point of contact on the CCR. The resulting curves are plotted in Fig. 10b for comparison. For all cases, the average error in prediction is less than 0.9 gram.

5. Discussion

The developed framework is able to predict the pose of the CCR with maximum error of 0.75% of the total length of the CCR. All the numerical procedures are conducted by

²The least count of load cell is 1 gram. Each measurements were repeated 6 times and the mean value rounded off to first decimal place is shown in the table.

gradually increasing the cable contraction through small incremental steps. As expected, the convergence of problems with obstacles is slower compared to those without obstacles. However, the time taken for convergence for a single obstacle and two obstacles is almost the same. For the `fmincon` procedure presented in this paper, the authors did not manually specify the gradient of objective function. We believe that by specifying the gradient, the convergence time could be further reduced.

The deviation between theoretical and experimental results for static analysis could be due to measurement errors from the experimental set-up. Possible sources of errors are cable extensions under large weights, friction between the discs and cable and dimensional inaccuracy arising from the surface finish of the 3D printed prototype. It should also be mentioned that the proposed method for static analysis does not take into account the material properties of the CCR and also does not derive its equations from elastic equilibrium equations. Hence, it is not possible to know the stress state of the system using this method, which is one of its disadvantages.

If two non-opposing cables are actuated simultaneously, the CCR bends in a plane which lies in between the two bending planes generated by pulling the two cables individually. The optimization-based kinematics formulation can be extended to such 3-D cases by minimizing the slope angles in both the individual bending planes. This is equivalent to minimization of total strain energy which consists of two strain energy components corresponding to the two bending directions. If \mathbf{x}_b represents the co-ordinates on the second cable and l_b is the length of a segment in the second cable, we can write the optimization problem as follows:

$$\arg \min_{\mathbf{x}_0, \mathbf{x}_a, \mathbf{x}_b} \sum_{i=0}^{n-1} \left[\left(\arccos \left(\frac{\mathbf{x}_0^{i+1} - \mathbf{x}_a^{i+1}}{\|\mathbf{x}_0^{i+1} - \mathbf{x}_a^{i+1}\|} \cdot \frac{\mathbf{x}_0^i - \mathbf{x}_a^i}{\|\mathbf{x}_0^i - \mathbf{x}_a^i\|} \right) \right)^2 + \left(\arccos \left(\frac{\mathbf{x}_0^{i+1} - \mathbf{x}_b^{i+1}}{\|\mathbf{x}_0^{i+1} - \mathbf{x}_b^{i+1}\|} \cdot \frac{\mathbf{x}_0^i - \mathbf{x}_b^i}{\|\mathbf{x}_0^i - \mathbf{x}_b^i\|} \right) \right)^2 \right]$$

Subject to:

$$\begin{aligned} \|\mathbf{x}_0^i - \mathbf{x}_0^{i-1}\| &= l_0, \quad \|\mathbf{x}_a^i - \mathbf{x}_a^{i-1}\| = l_a, \quad \|\mathbf{x}_b^i - \mathbf{x}_b^{i-1}\| = l_b \\ \|\mathbf{x}_0^i - \mathbf{x}_b^i\| &= a, \quad \|\mathbf{x}_0^i - \mathbf{x}_a^i\| = a, \\ \arccos \left(\frac{\mathbf{x}_a^i - \mathbf{x}_0^i}{\|\mathbf{x}_a^i - \mathbf{x}_0^i\|} \cdot \frac{\mathbf{x}_b^i - \mathbf{x}_0^i}{\|\mathbf{x}_b^i - \mathbf{x}_0^i\|} \right) &= \arccos \left(\frac{\mathbf{X}_a^i - \mathbf{X}_0^i}{\|\mathbf{X}_a^i - \mathbf{X}_0^i\|} \cdot \frac{\mathbf{X}_b^i - \mathbf{X}_0^i}{\|\mathbf{X}_b^i - \mathbf{X}_0^i\|} \right) \\ \mathbf{f}(\mathbf{x}_0) &\geq 0, \quad \mathbf{f}(\mathbf{x}_a) \geq 0, \quad \mathbf{f}(\mathbf{x}_b) \geq 0 \end{aligned} \tag{13}$$

$$i = 1, 2, 3, \dots, n$$

Given data: $\mathbf{X}_0, \mathbf{X}_a, \mathbf{X}_b, l_0, l_a, l_b, a, \mathbf{f}(\mathbf{x})$

The extra constraint on the angles between the vectors \mathbf{x}_a and \mathbf{x}_b ensure that the position of the holes remain fixed during bending. Simulated results for the bending of CCR in 3D is shown in Fig. 11. Accurate measurement of the CCR pose in 3D as well as estimating the three dimensional contact forces to validate the theoretical solution is a work currently underway.

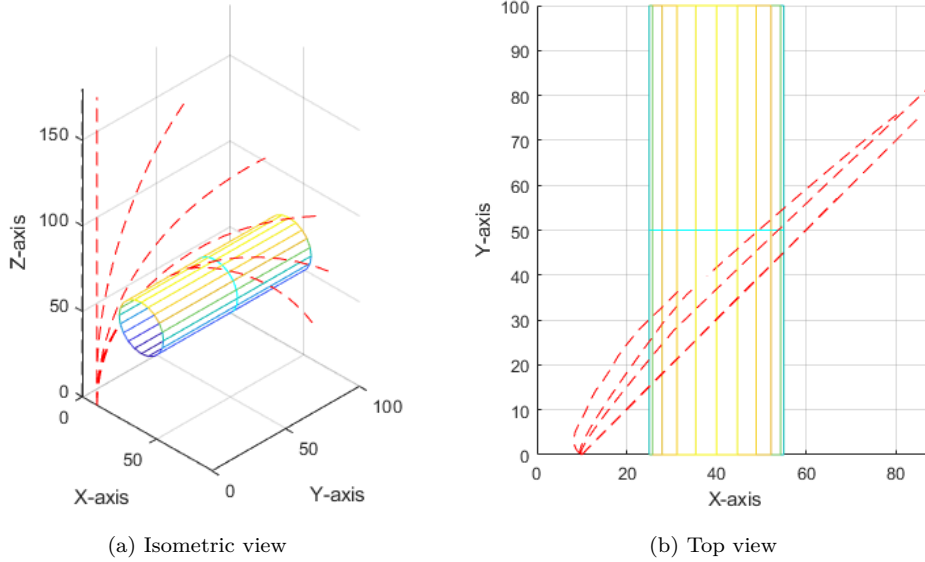


Figure 11: Trajectory of CCR in 3-D where two cables are actuated by equal amounts.

6. Conclusions and future work

In this paper, an optimization-based framework for the kinematics of cable-driven continuum robots is presented. The framework is derived from the minimum strain-energy principle and is experimentally shown to be accurate for predicting the deformed pose of a robot with 0.75% error. In the developed method, presence of obstacles can be directly incorporated to the optimization problem as inequality constraints. It is also not necessary to know the contact location of the obstacle beforehand for solving the kinematics which is an advantage of this approach as opposed to existing methods. The solution from experiments show that the framework gives the pose of a CCR with an error of 0.58% in presence of single and multiple obstacles. It is also shown that the contact location can be obtained by observing the Lagrange multipliers of the inequality constraints in the optimization problem. Using the kinematics, a simplified approach to estimate the contact forces using the method of virtual work is demonstrated. The statics analysis is shown to estimate the contact forces with average error of less than 0.9 grams.

The kinematic model can be extended to 3D motion of the CCR when two cables are actuated. Development of 3D force measurement for the 3D contact is a work in progress. Improving the model to reduce the computation time for real-time implementation in control systems is also a work in progress.

Acknowledgement

The 3D printing of the CCR was done at the Design and Innovation Center (DIC), UTSAAH Laboratory both at the Centre for Product Design and Manufacturing and at

the Makery Lab at the Robert Bosch Centre for Cyber Physical Systems. The authors thank the help provided at these labs.

References

- Ashwin, K.P., Chaudhury, A., Ghosal, A., 2020. Efficient representation of ducts and cluttered spaces for realistic motion planning of hyper-redundant robots through confined paths. *Computer-Aided Design* 119, 102777.
- Ashwin, K.P., Ghosal, A., 2021. Forward kinematics of cable-driven continuum robot using optimization method, in: *Mechanism and Machine Science*. Springer, pp. 391–403.
- Camarillo, D.B., Milne, C.F., Carlson, C.R., Zinn, M.R., Salisbury, J.K., 2008. Mechanics modeling of tendon-driven continuum manipulators. *IEEE Transactions on Robotics* 24, 1262–1273.
- Chirikjian, G.S., 2015. Conformational modeling of continuum structures in robotics and structural biology: A review. *Advanced Robotics* 29, 817–829.
- Dehghani, M., Moosavian, S.A.A., 2013. Static modeling of continuum robots by circular elements, in: 2013 21st Iranian Conference on Electrical Engineering (ICEE), IEEE. pp. 1–6.
- Do, T., Tjahjowidodo, T., Lau, M., Phee, S., 2015. A new approach of friction model for tendon-sheath actuated surgical systems: Nonlinear modelling and parameter identification. *Mechanism and Machine Theory* 85, 14–24.
- Gravagne, I.A., Rahn, C.D., Walker, I.D., 2003. Large deflection dynamics and control for planar continuum robots. *IEEE/ASME transactions on mechatronics* 8, 299–307.
- Khoshnam, M., Patel, R.V., 2013. A pseudo-rigid-body 3r model for a steerable ablation catheter, in: 2013 IEEE International Conference on Robotics and Automation, IEEE. pp. 4427–4432.
- Menon, M.S., Ananthasuresh, G., Ghosal, A., 2013. Natural motion of one-dimensional flexible objects using minimization approaches. *Mechanism and Machine Theory* 67, 64–76.
- Mishra, A.K., Mondini, A., Del Dottore, E., Sadeghi, A., Tramacere, F., Mazzolai, B., 2018. Modular continuum manipulator: analysis and characterization of its basic module. *Biomimetics* 3, 3.
- Rao, P., Peyron, Q., Lilge, S., Burgner-Kahrs, J., 2021. How to model tendon-driven continuum robots and benchmark modelling performance. *Frontiers in Robotics and AI* 7, 223.
- Robinson, G., Davies, J., 1999. Continuum robots - a state of the art, in: *Proceedings of the 1999 IEEE International Conference on Robotics and Automation, ICRA99*, pp. 2849–2854. 1999 IEEE International Conference on Robotics and Automation, ICRA99 ; Conference date: 10-05-1999 Through 15-05-1999.
- Rucker, D.C., Webster III, R.J., 2011. Statics and dynamics of continuum robots with general tendon routing and external loading. *IEEE Transactions on Robotics* 27, 1033–1044.
- Ryu, H.T., Woo, J., So, B.R., Yi, B.J., 2020. Shape and contact force estimation of inserted flexible medical device. *International Journal of Control, Automation and Systems* 18, 163–174.
- Venkateswaran, V.K., Sikorski, J., Misra, S., 2019. Shape and contact force estimation of continuum manipulators using pseudo rigid body models. *Mechanism and Machine Theory* 139, 34–45.
- Walker, I.D., 2013. Continuous backbone continuum robot manipulators. *International Scholarly Research Notices* 2013.
- Walker, I.D., Choset, H., Chirikjian, G.S., 2016. Snake-like and continuum robots, in: *Springer Handbook of Robotics*. Springer, pp. 481–498.
- Webster III, R.J., Jones, B.A., 2010. Design and kinematic modeling of constant curvature continuum robots: A review. *The International Journal of Robotics Research* 29, 1661–1683.